Appl. Phys. B 76, 597–602 (2003)
DOI: 10.1007/s00340-002-1085-3

Applied Physics B
Lasers and Optics

C. MOREAU[1]
E. THERSSEN[1,✉]
P. DESGROUX[1]
J.F. PAUWELS[1]
A. CHAPPUT[2]
M. BARJ[2]

Quantitative measurements of the CH radical in sooting diffusion flames at atmospheric pressure

[1] Physicochimie des Processus de Combustion et de l'Atmosphère – UMR 8522, FR CNRS 2416 CERLA, Université des Sciences et Technologies de Lille, 59655 Villeneuve d'Ascq Cedex, France
[2] Laboratoire de Spectrochimie Infrarouge et Raman – UMR 8516, FR CNRS 2416 CERLA, Université des Sciences et Technologies de Lille, 59655 Villeneuve d'Ascq Cedex, France

Received: 4 March 2002/Revised version: 5 November 2002
Published online: 5 May 2003 •

ABSTRACT The potential of Laser Induced Fluorescence detection of the CH radical using $C-X$ (0–0) excitation is investigated in a sooting methane/air diffusion flame at atmospheric pressure. Fluorescence is detected using the very narrow (< 0.4 nm) Q-branch of the $C-X$ (0–0) band, which enables the measurement of CH in sooting flames without interference from PAH fluorescence and soot emissions. Absolute concentrations are obtained using Cavity Ring Down Spectroscopy. 1D CH profiles in the sooting zone are recorded using a CCD camera with an excellent signal-to-noise ratio. The $C-X$ (0–0) excitation associated with Q-branch detection is shown to be three times more efficient than the $B-X$ scheme.

PACS 33.50.-j

1 Introduction

The detection of the CH radical in combustion processes is an important task, since this radical is a key reactant in the formation of prompt NO [1] and in the removal of NO via reburning [2]. In addition, CH is implicated in soot formation in hydrocarbon flames. This species exists in a relatively narrow spatial and temperature region of the flame and therefore experimental data concerning the CH radical provide very sensitive tests of chemical mechanisms for pollutant formation. Its detection also allows the flame fronts of turbulent flames to be located [3]. Because of the very low level of CH in flames (mole fraction of a few ppm), its detection requires highly sensitive techniques having good spatial resolution, like laser induced fluorescence (LIF).

Different LIF excitation/detection schemes for CH have been used, owing to the existence of three available electronic transitions in the UV and visible regions: the $A-X$ system near 430 nm, which suffers from a strong off-resonance signal [4–7], the $B-X$ system near 390 nm [3, 7, 8], and the $C-X$ system near 315 nm [9–11].

Since the C state is predissociated, most measurements have been achieved using the first two systems in view of obtaining a higher fluorescence quantum yield, which is defined as $\Phi = A/(A+Q+p)$, where A is the Einstein coefficient for spontaneous emission, Q the electronic quenching rate, and p the predissociation rate. A review of the different schemes, with their advantages and drawbacks, has recently been published by Luque et al. [12]. The choice of the spectroscopic scheme depends on the flame conditions, the major difficulty being avoiding the perturbation of Rayleigh and Mie scattering, because of the spectral proximity of the excitation and emission wavelengths, and preventing the saturation of the detector due to the flame emission. This difficulty is magnified by the fact that the LIF signal produced by CH relaxation is very weak. The second important point to consider concerns the variation of the fluorescence quantum yield with the flame conditions (temperature, pressure, and composition). Quantitative CH measurements require this variation to be taken into account, particularly for applications at atmospheric pressure [13].

In order to minimize the sensitivity of LIF measurements to quenching variations, some authors recommend the excitation of predissociated levels despite their associated low fluorescence quantum yield. Collisional deactivation of CH ($C^2\Sigma^+$) to CH ($A^2\Delta$) and CH ($B^2\Sigma^-$) has been observed (approximately 10%) and used successfully to detect CH by LIF in various atmospheric pressure flames [14]. Luque et al. [12] have demonstrated that the excitation of the predissociated $B^2\Sigma^- v' = 1$, $N' = 8$ level of CH is well suited for quantitative applications at atmospheric pressure. Previously, the $C^2\Sigma^+$ electronic state of CH has been probed near 312 nm and detection was achieved at 430 nm after $C \rightarrow A$ electronic energy transfer (EET) [9, 14, 15]. After that, Tsujishita et al. [10] obtained nice single-shot images of CH in atmospheric turbulent flames using the $C^2\Sigma^+$ $(v' = 1) \leftarrow X^2\Pi$ $(v'' = 0)$ excitation near 290 nm. The detection was achieved by collecting the $C^2\Sigma^+$ $(v' = 1) \rightarrow X^2\Pi$ $(v'' = 1)$ around 315 nm. They also tested the $C^2\Sigma^+$ $(v' = 0) \leftarrow X^2\Pi$ $(v'' = 0)$ excitation associated with the collection of the $C^2\Sigma^+$ $(v' = 0) \rightarrow X^2\Pi$ $(v'' = 1)$, but this scheme was found to be less efficient because of the off-diagonal detection. In both experiments, excitation and detection were well separated because of the use of different schemes (diagonal or off-diagonal) for excitation or detection. To our knowledge, this scheme has not been investigated further.

In this work, we have reconsidered the promising $C-X$ excitation by proposing an original and very efficient excitation/

✉ Fax: +33-3/2033-6463, E-mail: eric.therssen@univ-lille1.fr

detection scheme with a view to making quantitative CH measurements in sooting flames at atmospheric pressure. Indeed, in contrast to the other electronic schemes, the $C-X$ transition lies in a spectral region which is interference free from the wide and intense flame emission that occurs in the presence of polycyclic aromatic hydrocarbons (PAH) and soot (flame emission at 315 nm is much lower than that at 430 nm and a few times lower than that at 390 nm). Furthermore the excitation of the predissociated C state leads to moderately sensitive measurements of quenching variations. In this work, the CH radical was excited using the $P_1(10)$ line of the $C-X$ (0, 0) band around 317 nm and the fluorescence was detected on the intense Q-branch of the $C-X$ (0, 0) band at 314.4 nm. This scheme is particularly well suited to atmospheric pressure flame applications and competes well with the commonly used excitations ($A-X$ or $B-X$), which are affected by a large collisional quenching at high pressure. The fluorescence quantum yield of the $C-X$ excitation/detection scheme is shown to be at least as efficient as the $B-X$ (0, 0) system for quenching values higher than $7 \times 10^7\ \mathrm{s}^{-1}$. 1D spatially resolved detection of CH was obtained using a CCD camera at the exit plane of a spectrograph with an excellent signal-to-noise ratio, even in sooting flames.

This excitation/detection system was tested in two laminar flames of methane, a non-sooting and a sooting flame, and is shown to be very efficient, particularly in sooting flames because the detection is free from interference due to PAH and soot emission in the flame. Experiments were performed in atmospheric pressure diffusion flames stabilized on a three-slot Wolfhard–Parker burner. Relative CH profiles were calibrated by cavity ring down (CRD) measurements performed in an earlier work [11]. Such results are very important for the understanding reaction mechanisms in sooting flames. LIF measurements of radicals are scarce and there is concern about the OH radical in the oxidation zone of sooting flames [16–18]. To our knowledge, we report here the first quantitative CH measurements in sooting flames.

2 Experimental setup

Figure 1 shows a schematic diagram of the burner apparatus and of the optical setup used for the fluorescence measurements. A laminar methane/oxygen/nitrogen diffusion flame is stabilized on a Wolfhard–Parker (WP) burner at atmospheric pressure. A mixture of methane diluted in nitrogen flows from the central slots and a mixture of oxygen diluted in nitrogen flows from each of the two outside slots (Table 1). The slots are 4 mm wide and 30 mm long. This three-slot burner configuration (top view of the WP burner in Fig. 1) produces two identical vertical flame sheets 25–30 mm in length, which present approximately one dimensional characteristics in the parallel direction with the slots. A wire mesh

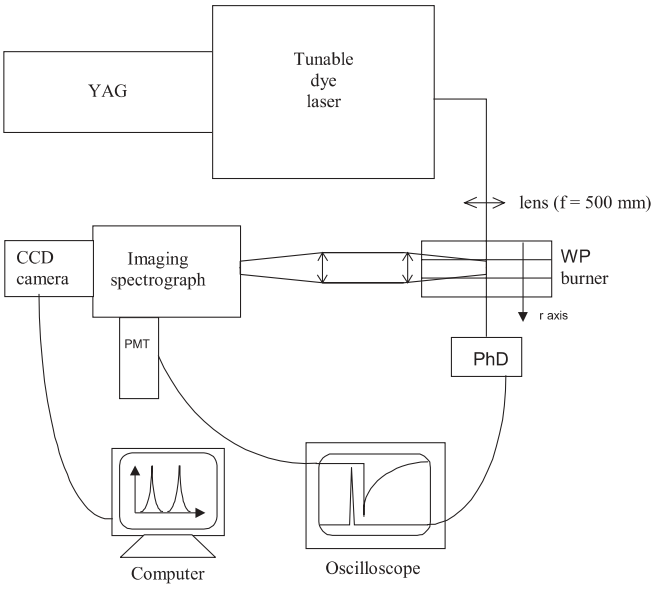

FIGURE 1 Experimental setup. The Wolfhard–Parker (WP) burner is schematically represented (*top view*). The r axis indicates the transverse direction of the WP burner. PhD: photodiode. PMT: photomultiplier tube

is placed at the burner top to stabilize the diffusion flame. The laser is aligned perpendicular to the slots (r axis). The symmetry about the burner centerline allows precise lateral profile data to be obtained in the r direction. These profiles can be recorded at different heights above the burner. According to their visual appearance, a non-sooting flame and a sooting flame were investigated. In the second flame, the soot was oxidized at the top of the burner leading to a non-smoking flame.

The laser system consists of a Quantel Nd:YAG laser pumping a dye laser with a bandwidth of $0.22\ \mathrm{cm}^{-1}$. The laser beam is focussed with a 500 mm focal length lens into the flame. The beam waist diameter is estimated to be around 300 μm and is nearly constant across the burner. Most of the measurements were performed with energies of a few mJ per pulse in a non-saturated LIF regime. A section of the laser beam 8 mm in length is imaged onto the entrance slit of a flat field spectrograph by a combination of two spherical lenses (200 mm focal length), providing 1 : 1 imaging. The spectrograph (ARC Spectrapro, 300 mm focal length, $f/4$, Czerny–Turner in line optical path) is equipped with a 2400 grooves/mm ruled grating. A Peltier-cooled intensified CCD camera (Princeton Instruments) is mounted in the exit focal plane of the spectrograph. The CCD camera has a 16 bit dynamic range. One dimension of the CCD-chip (576 columns) corresponds to the spectral axis, while the other one (384 rows) yields the spatial resolution along the imaged section (8 mm). This configuration enables spatial and spectral resolution of the fluorescence images. The temperature gradi-

TABLE 1 Mass flow rate conditions for the investigated methane diffusion flames. The mass flow rates are given at room temperature and atmospheric pressure

Flame number	Comment	% CH_4 in N_2	Q_{CH_4} ($\mathrm{L\,min^{-1}}$) central slot	Q_{N_2} ($\mathrm{L\,min^{-1}}$)	Q_{O_2} ($\mathrm{L\,min^{-1}}$) 2 outside slots	Q_{N_2} ($\mathrm{L\,min^{-1}}$)
1	non-sooting	20	0.29	1.15	2.16	2.16
2	sooting	40	0.58	0.86	2.16	2.16
3	high sooting	80	1.15	0.29	2.16	2.16

ent, which might perturb the propagation of the fluorescence photons between the laser axis and the CCD, was not found to distort the collected LIF images. Finally, a head-on photomultiplier tube (Philips XP2020Q), which is adjustable, is placed at the output slit to provide a bandpass adapted to the fluorescence band under investigation. The PMT signal is digitized and stored by an oscilloscope (Tektronix DSA 602A, 1 GHz bandwidth, 1 GS/s sampling rate) and later saved to a microcomputer in order to record the LIF excitation spectra and to test the fluorescence regime.

3 Excitation and detection conditions

In this section, the characteristics of the selected $C-X$ excitation/detection scheme of the CH radical are detailed, particularly in terms of the signal-to-noise ratio in hostile environments. A comparison with the commonly used excitation schemes is also provided.

3.1 *Quantum yield*

The quantum yield of fluorescence $\Phi = A/(A + Q + p)$ of predissociated states is very weak since the predissociation rate (p) is several orders of magnitude greater than the emission rate (A). A predissociation lifetime for $C-X$ ($v = 0$) levels was proposed by Brzozowski et al. [19] assuming the theoretical value for the radiative lifetime is equal to 89 ns [20]. They deduced a predissociation lifetime of about 10 ns for the lowest rotational levels. More recently, the lifetime of the $C^2\Sigma^+$ $v = 0$ state was calculated from linewidth measurements made under low pressure conditions (0.1 mbar) and was estimated to be around 4 ns [21]. Hirano et al. [9] assumed that the quenching time constant for the C state is 1–2.5 ns at atmospheric pressure. Quenching rates recorded in low pressure methane flames have been reported by Tamura et al. [13]. The rates across the flame range between 8×10^6 and $10 \times 10^6\ s^{-1}$ for the $A^2\Delta$ ($v' = 0$) state. The extrapolation of these experimental results to atmospheric pressure gives a quenching rate of about $2.5 \times 10^8\ s^{-1}$.

In view of comparing the efficiency of different excitation schemes for CH, we report in Table 2 their radiative lifetimes, collisional free lifetimes, and fluorescence quantum yields taken from LIFBASE [22] for the rotational level $N' = 11$. Two different collisional conditions were investigated: one at zero pressure ($Q = 0$) and one at atmospheric pressure, where the quenching rate was set to $2.5 \times 10^8\ s^{-1}$ according to the extrapolation mentioned before. In the case of the A and B states, p was set to zero while for the C state, the predissociation rate was calculated to be $2.4 \times 10^8\ s^{-1}$ ($v' = 0$) and $4.9 \times 10^8\ s^{-1}$ ($v' = 1$). It can be seen that the $C-X$ (0, 0) quantum yield is the highest at atmospheric pressure. Considering that the LIF signal is proportional to $B_{ij}\Phi$, it turns out that the $C-X$ (0, 0) excitation/detection scheme is about 3 times more efficient than the commonly used $B-X$ (0, 0) scheme at atmospheric pressure. Moreover, the predissociation rate that affects the C ($v' = 0$) state leads to less quenching sensitive LIF measurements (2 times less sensitive than the B and A states). One could limit this dependence by using the $C-X$ (1, 0) band and collecting the Q (1, 1) branch. However, this scheme suffers from a lower quantum yield compared to that of the $C-X$ (0, 0) band.

3.2 *Excitation transition*

The detection of the C state of CH by laser induced fluorescence suffers from interference due to OH fluorescence in the 310–320 nm spectral region corresponding to the $A-X$ band. Figure 2a shows an excitation LIF spectrum recorded by collecting the LIF signal near (314 ± 1) nm at a 3 mm height above the burner (HAB), where the laser beam crosses through the two flame fronts. The simulated spectra of OH and CH were obtained from LIFBASE [22]. The two simulated spectra, which were added and scaled arbitrarily, are presented in Fig. 2b. By comparing both the simulated and experimental spectra, the isolated CH lines emerge distinctly and can be assigned to the $P_1(10)$ and $P_2(10)$ lines at 317.3 nm. Finally, the CH profiles were obtained by exciting the $P_1(10)$ line of the $C-X$ (0–0) band at 317.3 nm

Band	Branch	A (s^{-1}) for $N' = 11$	B ($m^2\,J^{-1}\,s^{-1}$) for $N'' = 10$	T_r (ns)	T_p (ns)	Φ at $P = 0$ atm ($Q = 0$)	Φ at $P = 1$ atm ($Q = 2.5 \times 10^8\ s^{-1}$)	$B_{ij}\Phi$ at $P = 1$ atm ($m^2J^{-1}s^{-1}$)
$A-X$ (0, 0)	P	3.3×10^5	5×10^9	540	540	1	0.007	3.5×10^7
	Q	8×10^5	1.4×10^{10}					
	R	5.8×10^5	9.8×10^9					
$B-X$ (0, 0)	P	7.5×10^5	8.5×10^9	370	370	1	0.011	8.5×10^7
	Q	1.3×10^6	1.6×10^{10}					
	R	5.7×10^5	7.3×10^9					
$C-X$ (0, 0)	P	2.5×10^6	1.4×10^{10}	112	4	0.036	0.018	2.5×10^8
	Q	4.4×10^6	2.8×10^{10}					
	R	2×10^6	1.3×10^{10}					
$C-X$ (1, 0)	P	3.9×10^3	1.8×10^7	124	2	0.016	0.011	1.2×10^5
	Q	1.4×10^4	6.8×10^7					
	R	1.1×10^4	5.7×10^7					
$C-X$ (1, 1)	P	2.2×10^6	1.3×10^{10}	124	2	0.016	0.011	1.4×10^8
	Q	4×10^6	2.5×10^{10}					
	R	1.8×10^6	1.2×10^{10}					

TABLE 2 Transition parameters of the $A-X$, $B-X$, and $C-X$ bands of the CH radical for rotational level $N' = 11$, according to LIFBASE [22]. (A: Einstein coefficient of spontaneous emission, B: Einstein coefficient of absorption, T_r: radiative lifetime, T_p: collisional free lifetime, Φ: fluorescence quantum yield, Q: quenching rate. T_r and T_p are given at $P = 0.00$ atm)

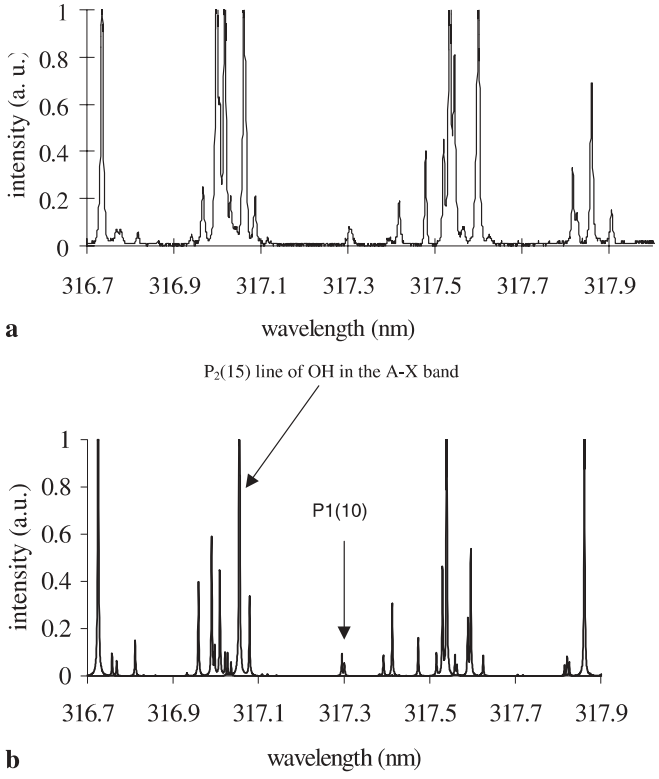

FIGURE 2 LIF excitation spectra of OH and CH radicals. **a** Experimental spectrum obtained at 3 mm (HAB) by collecting the fluorescence at (314 ± 1) nm. **b** Simulated spectra of OH and CH obtained by LIFBASE [22] at 1800 K using an arbitrary scaling factor

with a few mJ per pulse. At 3 and 7 mm HAB, a laser energy study showed that the LIF measurements were performed under non-saturated conditions. Rotational lines involving $N'' = 10$ have a small sensitivity to temperature variations. For a 1300–2000 K temperature range, the fractional population in $N'' = 10$ varies by ±5%.

3.3 *Detection band*

In Fig. 3, we show a simulated spectrum of the $C-X$ (0, 0) emission for the CH radical obtained by LIFBASE [22] at 1800 K. It can be seen that the Q-branch is very congested (< 0.4 nm). Thus, by selecting this appropriate spectral width on the CCD camera, a very efficient collection of the fluorescence (about 50% according to the A values in Table 2) can be obtained with a very high rejection of interference due to flame emission, PAH broadband fluorescence and OH fluorescence. Using this detection scheme, CH fluorescence profiles along the spatial dimension of the burner (r axis, 8 mm long) can be recorded at different heights above the burner with an excellent signal-to-noise ratio.

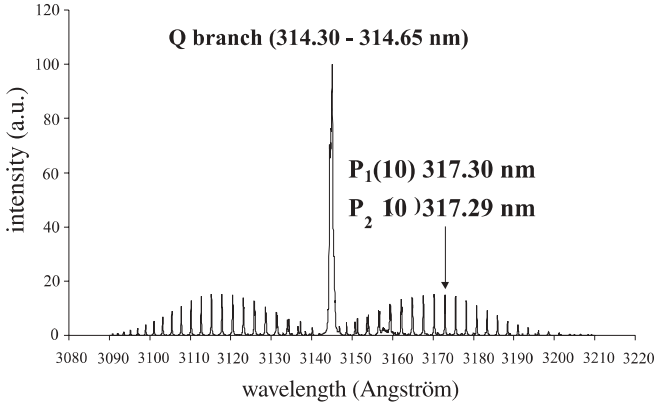

FIGURE 3 Simulated spectrum of CH emission for the $C-X$ (0, 0) band using LIFBASE [22] at 1800 K

4 Results and discussion

4.1 *In the non-sooting flame*

In a previous study [11], CH profiles were obtained by cavity-ring-down spectroscopy (CRDS) in a non-sooting diffusion flame. The CRD measurements were carried out by probing the $P_1(8)$ transition with the laser aligned with the burner slots. Figure 4a and b show the comparison between the LIF profiles recorded with a CCD camera and the CRD measurements at two heights above the burner, $h = 3$ and 6 mm, in the flame 1. The LIF measurements were performed by probing the $P_1(10)$ line of CH. The fluorescence was collected either using the Q-branch of the $C-X$ band or using the $A-X$ emission near 430 nm subsequent to the electronic energy transfers (EET) from the C state.

The variation of the Boltzmann fraction between the two experiments (LIF and CRDS) does not affect the shape of the CH profiles because of the narrow flame temperature range in which CH is present. The LIF profiles are narrower than those obtained by CRDS. Typically, the FWHM of the LIF

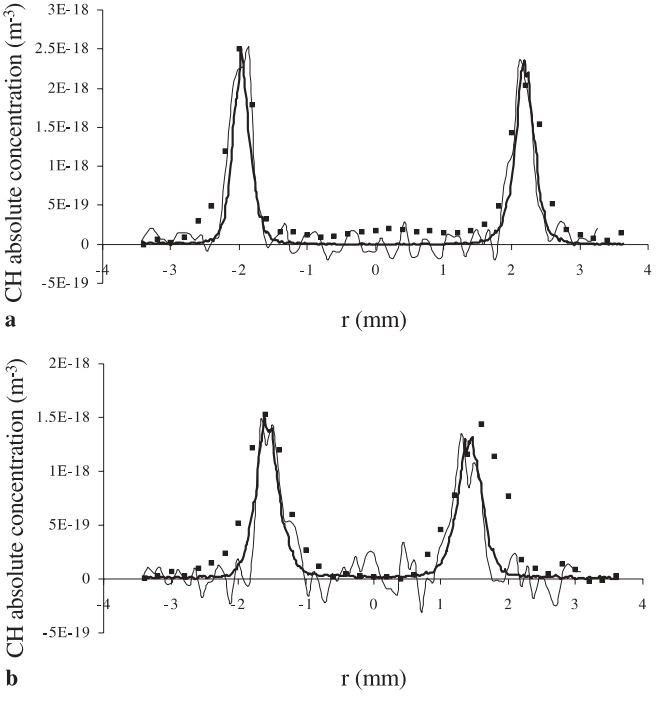

FIGURE 4 CH profiles obtained by LIF upon $P_1(10)$ excitation in the $C-X$ (0, 0) band. Collection was performed on the $C-X$ (0, 0) Q-branch (*bold solid line*) and after electronic energy transfer on the $A-X$ band (*thin solid line*). Profiles have been scaled in absolute value using previous CRDS measurements (*symbols*) [11]. The profiles were recorded at 3 mm (**a**) and 6 mm (**b**) above the burner in flame 1 (Table 1)

profile at $h = 6$ mm is approximately 1 mm. The difference is due to the lower spatial resolution of the spatially integrated CRD measurements. The same observation has been made previously [11].

However, good agreement between LIF and CRD profiles is found for the two heights above the burner. As CRD measurements are not affected by quenching, this agreement could indicate that the quenching variations across the flame are weak and do not affect the fluorescence quantum yield. This good agreement allows an absolute quantification of the profiles on the basis of CRDS measurements in the temperature range of the flame. The profiles were scaled in absolute concentration using the peak value of the CRDS profile at 3 mm [11]. The absolute peak concentration was found to be 2.5×10^{18} m^{-3} and corresponds to a mole fraction of 0.57 ppm.

From Fig. 4, the signal-to-noise ratio is shown to be much higher using the $C-X$ detection rather than the $A-X$ detection after EET. However, the good agreement between the shape and the magnitude of the CH profiles recorded using the two detection schemes indicates that EET is weakly affected by the change of the flame conditions with HAB and radial position.

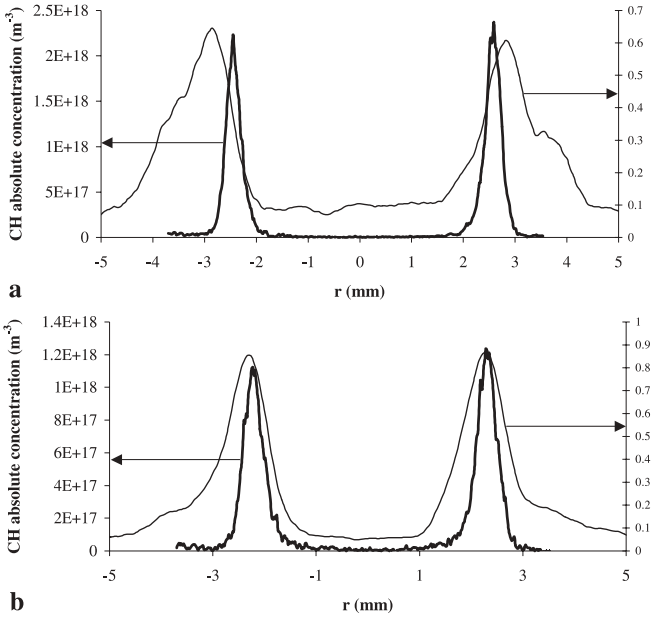

FIGURE 6 CH LIF profiles (*bold solid line*) obtained in the sooting flame 2 (Table 1) at $h = 3$ mm (**a**) and $h = 6$ mm (**b**). The flame emission at 650 mm (*thin solid line*) is given (arbitrary units on the right part) in order to locate the soot. The 650 nm emission profile at 3 mm has been magnified by a factor of 50 compared to that at 6 mm. The LIF profiles have been calibrated in absolute concentration using CRDS calibration in flame 1

4.2 *In sooting flame*

Figure 5 shows a 1D-spectral image recorded by the CCD camera/spectrograph detection system in the high sooting flame 3 (Table 1). This result was obtained in a sooting zone. Around 317 nm, elastic scattering is present along the laser beam, particularly in the sooting zone due to strong Mie and/or Rayleigh scattering from soot particles. For shorter wavelengths, the spectrum only exhibits the intense Q- and R-branches of $C-X$ CH fluorescence. Figure 6 shows CH profiles in the sooting flame 2 (Table 1) obtained by selecting a bandwidth corresponding to the Q-branch.

Because of the weak quenching dependence of $C-X$ LIF measurements, the calibration via CRD measurements used first for flame 1 (non-sooting flame) was applied to flame 2 (sooting flame).

In order to locate the soot, we recorded the flame emission at 650 nm. The intensity at $h = 3$ mm is magnified by a factor of 50. The remaining signal in the middle and outside the burner was due to the gas emission at this wavelength. Even in the presence of soot, the CH radical surrounding the particles was detected with an excellent signal-to-noise ratio. Preliminary results indicate that the CH concentration and its consumption in the early steps of soot formation are very close to those obtained in the non-sooting flame.

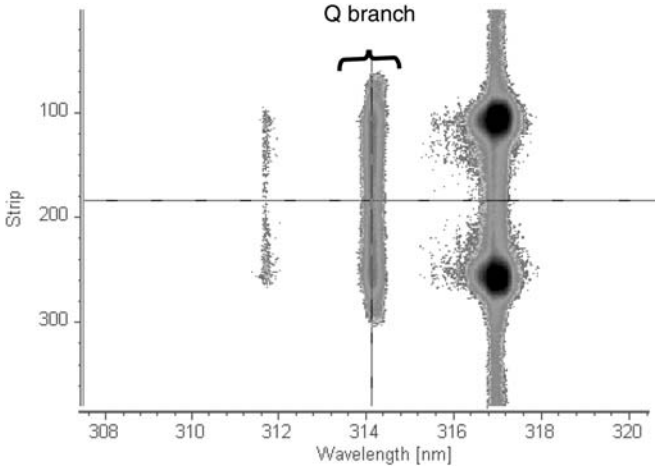

FIGURE 5 1D-spectral LIF image of CH radical recorded by the CCD/spectrograph detection system in the high sooting flame 3 (Table 1). The excitation wavelength was near 317 nm in order to probe the $P_1(10)$ line in the $C-X$ (0, 0) band

5 Conclusion

We have demonstrated the high potential of the $C-X$ (0, 0) excitation/detection system, which is particularly attractive for the study of hostile media like sooting flames. The Q-branch shows a very narrow bandwidth (< 0.4 nm) and is sufficiently separated from the excitation wavelength. These characteristics make the $C-X$ (0, 0) excitation/Q detection system very efficient and totally free from interference from the background signal (LIF from different species, flame emission, PAH fluorescence, Rayleigh and Mie scattering). The good agreement between CRD and LIF spatial profiles across the flame front suggests that the variation of quenching from the C state should not noticeably affect the fluorescence in the studied flame. This information confirms the quantitative features of CH LIF imaging performed with the $C-X$ (0, 0) excitation/detection scheme. In different flames (with or without soot), the profiles for CH exhibit very good signal-to-noise ratios. Further work will concern (1) simultaneous detection of OH and CH using a single laser around 317 nm and (2) obtaining 2D images of CH in sooting flames

using the selected excitation scheme and a narrow band filter centered at 314 nm.

ACKNOWLEDGEMENTS We gratefully thank L.R. Sochet for triggering this project of an imaging detection system applied to a diffusion flame. The "Laboratoire de Cinétique et Chimie de la Combustion – UMR 8522" and The "Laboratoire de Spectrochimie Infrarouge et Raman – UMR 8516" are "Unité Mixte de Recherche de l'Université de Lille 1 et du CNRS". The Centre d'Etudes et de Recherches Lasers et Applications (CERLA) is supported by the Ministère de la Recherche, the Région Nord-Pas de Calais, and the Fonds Européen de Développement Economique des Régions.

REFERENCES

1 J.A. Miller, C.T. Bowman: Prog. Energy Combust. Sci. **15**, 287 (1989)
2 T. Kolb, P. Jansohn, W. Leuckel: 22nd Symp. (Int.) Combust. (The Combustion Institute, Pittsburgh 1988) p. 1193
3 C.D. Carter, J.M. Donbar, J.F. Driscoll: Appl. Phys. B **66**, 129 (1998)
4 T.S. Norton, K.C. Smyth: Combust. Sci. Technol. **76**, 1 (1991)
5 R.J. Cattolica, D. Stepowski, D. Puechberty, M. Cottereau: J. Quant. Spectrosc. Radiat. Transfer **32**, 363 (1984)
6 R.G. Joklik, J.W. Daily, W.J. Pitz: 21st Symp. (Int.) Combust. (The Combustion Institute, Pittsburgh 1986) p. 895
7 K.J. Rensberger, M.J. Dyer, R.A. Copeland: Appl. Opt. **27**, 3679 (1988)
8 K.A. Watson, K.M. Lyons, J.M. Donbar, C.D. Carter: Combust. Flame **117**, 257 (1999)
9 A. Hirano, M. Ippommastu, M. Tsujishita: Opt. Lett. **17**, 303 (1992)
10 M. Tsujishita, M. Ippommastu, A. Hirano: Jpn. J. Appl. Phys. **32**, 5564 (1993)
11 X. Mercier, P. Jamette, J.F. Pauwels, P. Desgroux: Chem. Phys. Lett. **305**, 334 (1999)
12 J. Luque, R.J.H. Klein-Douwel, J.B. Jeffries, D.R. Crosley: Appl. Phys. B **71**, 85 (2000)
13 M. Tamura, P.A. Berg, J.E. Harrington, J. Luque, J.B. Jeffries, G.P. Smith, D.R. Crosley: Combust. Flame **114**, 502 (1998)
14 J.B. Jeffries, R.A. Copeland, G. Smith, D.R. Crosley: 21st Symp. (Int.) Combust. (The Combustion Institute, Pittsburgh 1986) p. 1709
15 D.R. Crosley: Combust. Flame **78**, 153 (1989)
16 M. Haudiquert, A. Cessou, D. Stepowski, A. Coppalle: Combust. Flame **111**, 338 (1997)
17 A. Garo, G. Prado, J. Lahaye: Combust. Flame **79**, 226 (1990)
18 R. Puri, M. Moser, R.J. Santoro, K.C. Smyth: 24th Symp. (Int.) Combust. (The Combustion Institute, Pittsburgh 1992) p. 1015
19 J. Brzozowski, P. Bunker, N. Elander, P. Erman: Astrophys. J. **207**, 414 (1976)
20 J. Hinze, G. Lie, B. Liu: Ap. J. **196**, 621 (1975)
21 W. Ubachs, G. Meyer, J.J. ter Meulen, A. Dymanus: J. Chem. Phys. **84**, 3032 (1986)
22 J. Luque, D.R. Crosley: LIFBASE: Database and Spectral Simulation Program, Ver. 1.2, SRI International Report MP 98-021 (1998)